Journal of Power Sources 224 (2013) 86–92

Contents lists available at SciVerse ScienceDirect

Journal of Power Sources

journal homepage: www.elsevier.com/locate/jpowsour

Effect of temperature on the pseudo-capacitive behavior of freestanding MnO_2@carbon nanofibers composites electrodes in mild electrolyte

Jian-Gan Wang [a,b], Ying Yang [c,d], Zheng-Hong Huang [b], Feiyu Kang [a,b,*]

[a] State Key Laboratory of New Ceramics and Fine Processing, Department of Materials Science and Engineering, Tsinghua University, Beijing 100084, China
[b] Institute of Advanced Materials Research, Graduate School at Shenzhen, Tsinghua University, Shenzhen 518055, China
[c] Department of Electrical Engineering, Tsinghua University, Beijing 100084, China
[d] State Key Laboratory of Control and Simulation of Power System and Generation Equipments, Tsinghua University, Beijing 100084, China

HIGHLIGHTS

- Hierarchical δ-MnO_2 nanoflakes @carbon nanofibers composites are prepared.
- Effect of temperature on pseudo-capacitive behaviors is extensively studied.
- The composites show good electrochemical performance in range of 0–75 °C
- The δ-MnO_2 is found to evolve to γ-MnO_2 nanorods during cycling test at 75 °C.

ARTICLE INFO

Article history:
Received 18 July 2012
Received in revised form
16 September 2012
Accepted 19 September 2012
Available online 28 September 2012

Keywords:
Supercapacitor
Manganese oxide
Carbon nanofiber
Temperature effect
Aqueous electrolyte

ABSTRACT

Electrospun carbon nanotubes-embedded carbon nanofibers (CNF) fabric is employed as freestanding substrates for *in-situ* coating MnO_2 nanostructures. Birnessite-type MnO_2 nanoflakes are observed to grow vertically on individual CNF, thus building hierarchical coaxial architecture. This work presents an extensive study of the effect of temperature on the pseudo-capacitive behavior of the as-prepared freestanding MnO_2@CNF composites electrodes in mild Na_2SO_4 electrolyte. The results show that the MnO_2@CNF composites exhibit excellent pseudo-capacitive behaviors at different temperatures between 0 °C and 75 °C. The specific capacitance at 1 A g^{-1} increases from 365 F g^{-1} at 0 °C to 546 F g^{-1} at 75 °C, whereas the coulombic efficiency decreases with the increasing temperature, especially at lower charging rate. The cycling stability of the composites strongly depends on the temperature, *i.e.*, 95.3% at 25 °C and 82.4% at 75 °C. This study provides a fundamental understanding of the temperature-dependent capacitive properties of MnO_2 in mild electrolyte, which gives an insight into the supercapacitor design for industrial applications.

1. Introduction

Supercapacitors have been considered as promising energy storage devices due to their high power and energy densities, long cycling stability and safe operation [1,2]. According to the charge storage mechanism, supercapacitors can be categorized as electrical double-layer capacitors (EDLCs) using porous carbon materials and pseudocapacitors using redox-active materials [3,4]. In particular, pseudocapacitors based on transition metal oxides exhibit much higher specific capacitance than carbonaceous materials and better cycling stability than conducting polymers [5]. To date, great efforts have been devoted to these attractive candidates including RuO_2, MnO_2, Co_3O_4, NiO and V_2O_5, *etc* [6–8]. Among them, manganese oxides (MnO_2) are the most potential one because of their low cost, natural abundance, high theoretical capacity (~1370 F g^{-1}), non-toxicity and wide operating potential window in mild electrolyte [9,10]. However, bulk MnO_2 suffers from low electronic conductivity, low ionic diffusion constant and structural susceptibility. This stimulates an extensive interest on developing MnO_2-based composites with conductive materials, such as carbon nanotubes, graphene, carbon nanofibers and conducting polymers, *etc*., in order to overcome their drawbacks [11–15].

As energy storage devices, supercapacitors may operate in harsh temperature environments, such as low temperature in freezing winter and high temperature in electric vehicle. A systematic work of the temperature effects on the capacitive behavior is rather

* Corresponding author. State Key Laboratory of New Ceramics and Fine Processing, Department of Materials Science and Engineering, Tsinghua University, Beijing 100084, China. Tel./fax: +86 10 6279 2911.
E-mail address: fykang@tsinghua.edu.cn (F. Kang).

0378-7753/$ – see front matter © 2012 Elsevier B.V. All rights reserved.
http://dx.doi.org/10.1016/j.jpowsour.2012.09.075

desirable, however, until recently, most studies focused on their performance at room temperature and very few have done temperature-dependent studies. Gallay et al. and Soukiazian et al. have studied the electrochemical performance of activated carbon in 1 M Et_4NBF_4 in acetonitrile and propylene carbonate (PC) at the temperature between −40 °C and 70 °C [16,17]. Wei et al. presented the effect of temperature (25 °C—100 °C) on the capacitance of single-walled carbon nanotube film in organic $TEABF_4$/PC electrolyte [18]. Pickup et al. tested the performance of RuO_2 in H_2SO_4 electrolyte at the temperatures from −40 °C to 40 °C [19]. Lee et al. and our preliminary study discussed a temperature dependent capacitive behavior of MnO_2 in Na_2SO_4 electrolyte [20,21]. The specific capacitances of these active materials were demonstrated to decrease with decreasing temperature. The carbonaceous materials were also found to show excellent stability at various temperatures. It should be noted that the carbonaceous materials store energy by surface adsorption/desorption but MnO_2 depends mainly on reversible Faradic redox reaction. Hence, the origin of temperature effects on the pseudo-capacitive behavior of MnO_2 may be different from that of carbonaceous materials. Moreover, MnO_2 is not as stable as carbonaceous materials at high temperature, which may cause a phase transition and morphological change. Up to now, no reports have addressed these critical issues.

In this work, we employ a highly conductive electrospun carbon nanotubes (CNT) embedded carbon nanofibers (CNF) substrate for uniform coating hierarchical birnessite-type MnO_2 nanoflakes. The as-prepared MnO_2@CNF composites are used as freestanding electrodes to investigate the temperature effects on their electrochemical performance in mild Na_2SO_4 electrolyte. The freestanding nature of the composites avoids the disturbance of polymeric binders and conductive additives, which provides a better understanding of the pseudo-capacitive behavior of MnO_2. Cyclic voltammetry (CV), galvanostatic charging/discharging technique and electrochemical impedance spectroscopy (EIS) are used to extensively analyze the pseudo-capacitive behavior at different temperature between 0 °C and 75 °C. The cycling stability is studied to illustrate the structural and morphological evolution of MnO_2 at 25 °C and 75 °C.

2. Experimental

2.1. Synthesis of CNF/MnO_2 composites

Carbon nanotubes-embedded carbon nanofibers fabric was fabricated using high-voltage electrospinning technique as reported in Ref. [21]. Briefly, 0.5 wt.% of purified and functionalized carbon nanotubes was dispersed into 10 wt.% polyacrylonitrile (PAN, Mw = 150 K)/dimethyl formamide (DMF) solution to form a homogeneous precursor. The precursor was electrospun into a gray nonwoven cloth. CNF fabric was produced by hot pressing, preoxidation treatment (250 °C/2 h in air) and a final carbonization (1000 °C/2 h in nitrogen atmosphere) on the as-spun cloth. The CNF fabric was then tailored into 10 mm × 10 mm of square substrates as freestanding electrodes. The incorporation of MnO_2 nanostructures was conducted by immersing the square substrates into neutral $KMnO_4$ solution at 65 °C. The weight ratio of CNF to $KMnO_4$ was controlled to 2:1. The MnO_2@CNF fabric was taken out when the purple color of $KMnO_4$ had faded into golden brown. The obtained MnO_2@CNF composites were rinsed using deionized water for several times to remove the residual reactants and finally dried at 80 °C for 12 h.

2.2. Materials characterization

The morphology of the composites was observed on a field emission scanning electron microscopy (FESEM, LEO-1530). The crystallographic information of the products was investigated by powder X-ray diffraction (XRD, Rigaku D/Max 2500PC). The Raman spectrums were recorded on Renishaw Invia RM200 (England) at room temperature in the spectral range 200—2500 cm^{-1}. The laser

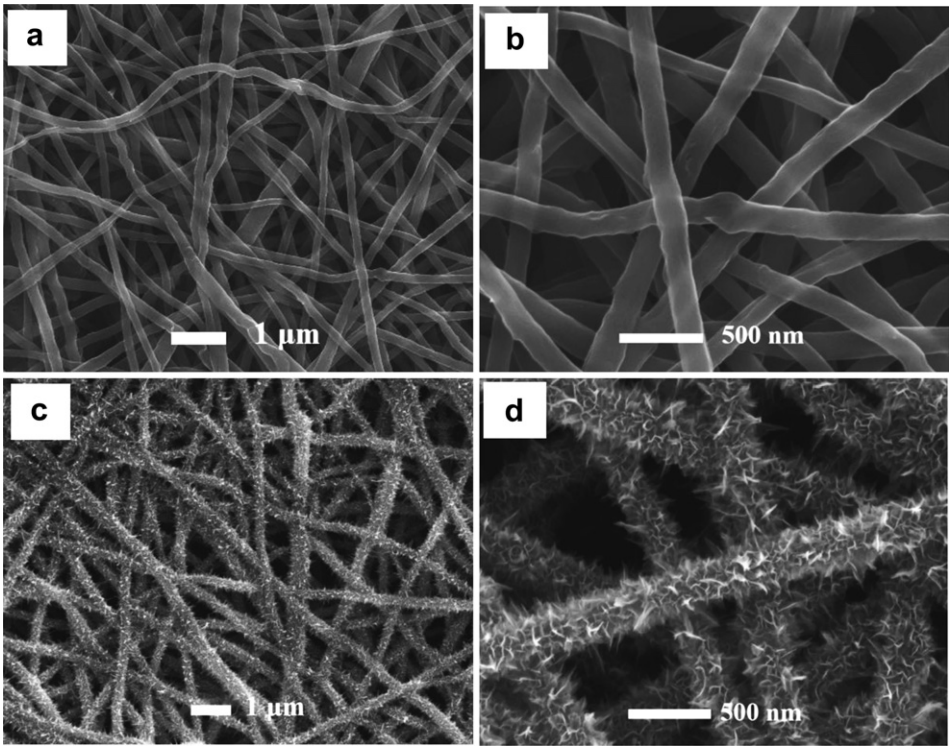

Fig. 1. SEM images of (a and b) the CNT-embedded CNF and (c and d) MnO_2@CNF composites.

light source was provided by the excitation of an argon-ion laser at a wavelength 514.5 nm. The ×50 objective lens of the microscope was used to focus the laser beam on a small selected area of the electrode. The mass content of MnO_2 coatings of CNF/MnO_2 composites was determined using thermogravimetric analysis (TGA, SDT-Q600).

2.3. Electrochemical measurements

The electrochemical performance of as-prepared composites as freestanding electrodes was carried out on the CHI 660B electrochemical station in a three-electrode configuration with platinum wire and saturated calomel electrode (SCE) as counter and reference electrode, respectively. The cyclic voltammetry (CV) and galvanostatic charging/discharging techniques were employed to investigate the electrochemical performance of the composites at different temperatures. The temperature was controlled to 0 °C, 25 °C, 50 °C and 75 °C. The applied potential window was ranged from −0.05 V to 0.85 V in a 0.5 M Na_2SO_4 electrolyte. The electrochemical impedance spectroscopy (EIS) was conducted in the frequency range between 100 kHz and 20 mHz with a perturbation amplitude of 5 mV versus the open-circuit potential. The average specific capacitances were calculated from the CVs and discharging curves according to the Eqs. (1) and (2), respectively.

$$C = \frac{1}{m \cdot v \cdot \Delta V} \int i(V) \mathrm{d}V; \quad (1)$$

$$C = \frac{I \cdot \Delta t}{m \cdot \Delta U}; \quad (2)$$

where, m is the mass of active materials, v is the potential scan rate, ΔV is the potential window in CV, $i(V)$ is the voltammetric current, I is the applied current, ΔU is potential window in discharging process and Δt is the discharging time.

3. Results and discussion

The controlled growth of nanostructured MnO_2 with desirable morphologies on different carbonaceous substrates is generally based on the redox reaction between carbon and permanganate ions (MnO_4^-), which can be written as follows: [22]

$$4MnO_4^- + 3C + H_2O \rightarrow 4MnO_2 + CO_3^{2-} + 2HCO_3^- \quad (3)$$

In this study, the electrospun CNTs-embedded CNFs are employed as both reducing agents and rigid backbones for MnO_2 growth. Fig. 1(a) and (b) presents the SEM images of the pristine nanofibers, showing a curled fibrous morphology with rough surfaces due to the embedding of CNTs. The diameter of the CNTs-embedded CNFs is in the range of 100–300 nm. It is demonstrated the incorporation of CNTs could increase the electronic conductivity of CNF from 11.6 S cm^{-1} to 24.1 S cm^{-1} [21]. The enhanced conductivity would facilitate the electron transfer rates during the charge storage processes and thus ensure a better utilization of MnO_2. Fig. 2(c) and (d) shows the morphology of MnO_2@CNF composites. The fibrous network with porosity and interconnectivity is preserved after MnO_2 deposition. Porous MnO_2 nanoflakes are observed to vertically grow on the external surfaces of CNF, building a hierarchical coaxial configuration. The MnO_2 nanostructures are also coated uniformly on individual nanofibers without any dissociative agglomerates. Such a hierarchical architecture could expose more electroactive surface area of MnO_2 available by the electrolyte, promoting a maximum harvest of psuedocapacitance.

The crystallographic structure of the MnO_2@CNF composites is investigated by XRD and Raman measurements. Fig. 2(a) and (b) shows the corresponding XRD pattern and Raman spectrum, respectively. As shown in the XRD pattern, the broad peaks with 2θ around 20°–30° and 40°–45° are ascribed to the (002) and (10) planes of amorphous carbon, which is consistent with the turbostratic structure of electrospun CNF [23]. In particularly, the sharp diffraction peak at $2\theta = 26°$ is an indication of the (002) plane of graphitic carbon, suggesting the presence of the embedded CNTs. In addition, the diffraction peaks at $2\theta = 12°$, 37° and 66° can be indexed to the (001), (111) and (020) reflections of birnessite-type

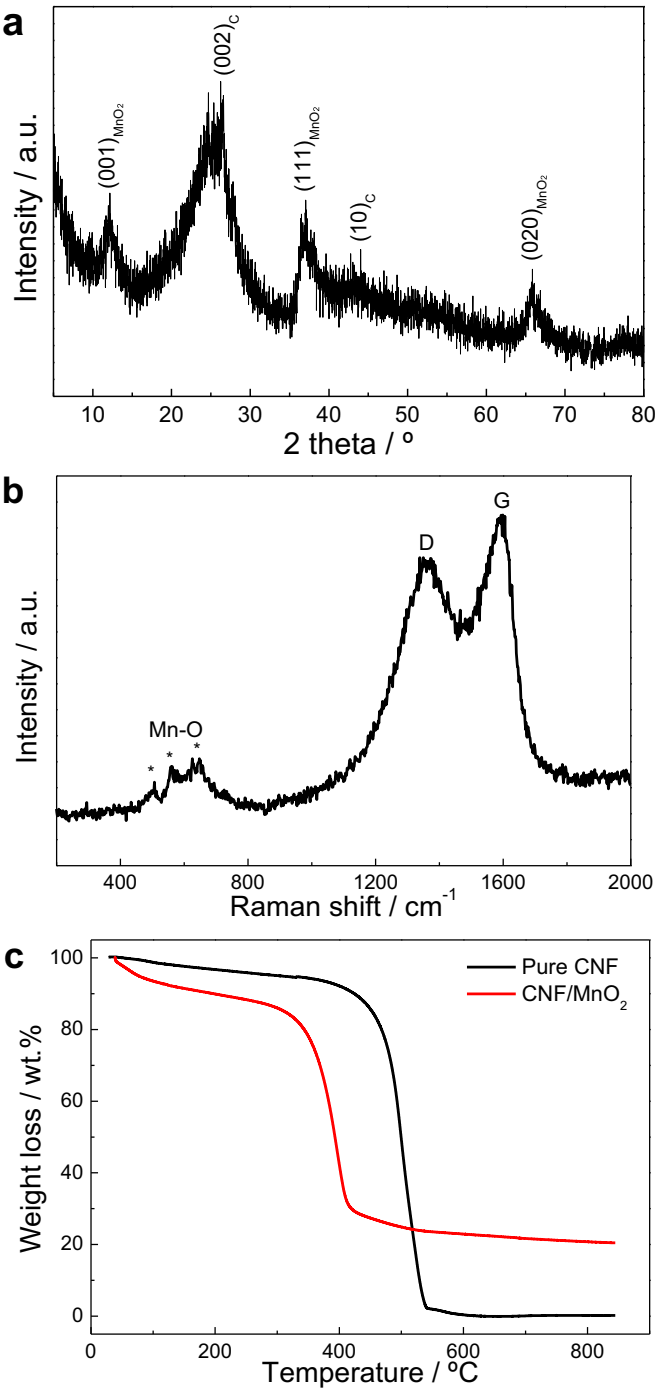

Fig. 2. (a) XRD pattern and (b) Raman spectrum of the as-prepared MnO_2@CNF composites. (c) TGA curves of pure CNF and MnO_2@CNF composites.

MnO_2 (JCPDS 42-1317) [24]. All the peaks from MnO_2 are broad and weak, indicating the nature of amorphous nanocrystals. The birnessite-type structure of MnO_2 is further confirmed by Raman analysis. As shown in Fig. 2(b), the sharp and strong G bands at 1580 cm^{-1} and the relatively weak D bands around 1350 cm^{-1} obviously come from the CNF. Besides the carbon peaks, the major Raman bands at 501 cm^{-1}, 575 cm^{-1} and 645 cm^{-1} are attributed to the Mn–O stretching vibration of [MnO_6] octahedra, the Mn–O stretching vibration in the basal plane of [MnO_6] sheets and the symmetric Mn–O stretching vibration of [MnO_6] group, respectively [25]. These Raman scattering results are in good agreement with the birnessite-type MnO_2 [26]. The mass content of MnO_2 coatings is determined by TGA, as shown in Fig. 2(c). The initial 10% weight loss up to 200 °C is attributed to the removal of adsorbed water in the composites. The following steep weight loss of 73% between 300 °C and 450 °C corresponds to the combustion of carbon species. The carbon-combustion temperature of CNF/MnO_2 is found to be lower than that of CNF in the absence of MnO_2, which is due to the catalytic function of Mn species [27]. The small weight loss of 2 wt.% above 500 °C is ascribed to the partial reduction of MnO_2 to Mn_3O_4 accompanied by oxygen evolution [28]. The mass content of MnO_2 is estimated to be 24 wt.% from the TGA curve, which is very close to the theoretical value (25.4 wt.%) calculated by using Equation (3).

Cyclic voltammogram (CV) was performed to evaluate the electrochemical capacitive behavior of the MnO_2@CNF composites at different temperatures of 0 °C, 25 °C, 50 °C and 75 °C Fig. 3(a) shows the CV curves recorded at the scan rate of 2 mV s^{-1}. Our previous study has demonstrated the capacitance is mainly from the MnO_2 nanoflakes [21]. All CV curves exhibit near-rectangular shapes without evident redox peaks, indicating the ideal pseudo-capacitive behaviors with highly reversibility at each set of temperatures. Notably, the leveled current density increases with the increasing temperature, suggesting a higher specific capacitance at higher temperature. However, it can be observed that the current response at high potential is deviated from the equilibrium state at high temperature, suggesting increasing temperature would lead to a significant electrochemical polarization during the charging process. This irreversible polarization may accelerate the reduction of MnO_2 to soluble Mn^{2+} and thus result in rapid capacitance degradation. Fig. 3(b) and (c) shows the CV curves of 0 °C and 75 °C at various scan rates. As the scan rate increasing from 2 mV s^{-1} to 50 mV s^{-1}, the rectangular shape of CV at 75 °C has a smaller distortion than that of CV at 0 °C, indicating better rate capability at higher temperature. The dependence of the specific capacitance (SC) on the scan rate is plotted in Fig. 3(d). At the temperature of 75 °C, the SC value of MnO_2@CNF composites reaches as high as 551 F g^{-1} at a low scan rate of 2 mV s^{-1}, which is increased by 45% in contrast to the value at 0 °C (380 F g^{-1}). The SC decreases with the increase in the scan rate. Two charge storage mechanisms of MnO_2 are proposed in mild Na_2SO_4 electrolyte, involving surface adsorption/desorption and bulk insertion/extraction of Na^+, which are expressed as Eqs. (4) and (5), respectively [9].

$$(MnO_2)_{surface} + Na^+ + e^- \leftrightarrow \left(MnO_2^- Na^+\right)_{surface} \quad (4)$$

$$MnO_2 + Na^+ + e^- \leftrightarrow MnOONa \quad (5)$$

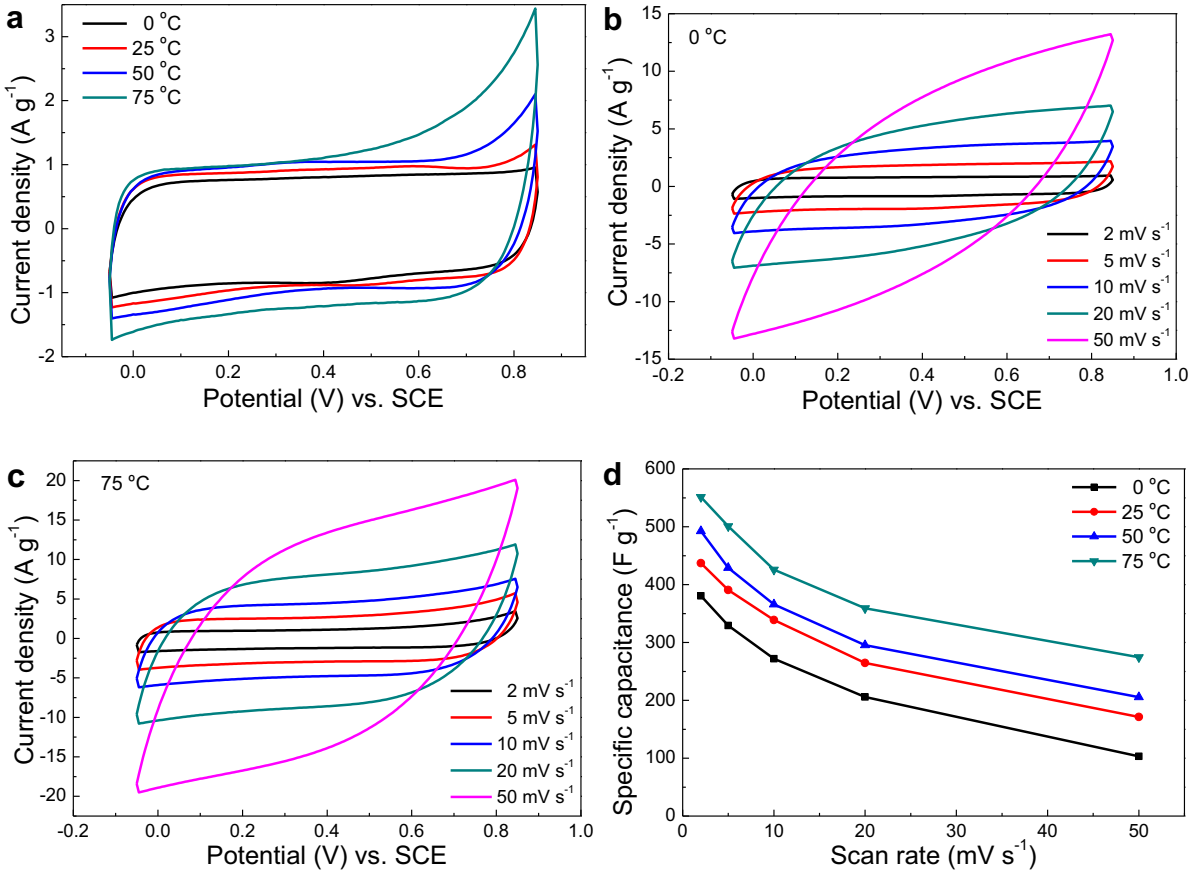

Fig. 3. CV curves of MnO_2@CNF composites (a) at different temperatures (scan rate: 2 mV s^{-1}) and at various scan rates tested at (b) 0 °C and (c) 75 °C. (d) Specific capacitance of the electrodes as a function of scan rate.

This suggests the diffusion of Na^+ into interior MnO_2 and the transfer of charges have a significant effect on the rate capability. At low scan rate, the ions in the electrolyte can diffuse sufficiently into the interior surfaces for more charge storage. The interior surfaces are difficult to be available by ions at high scan rates due to the reduced diffusion time, which leads to a low capacitance. Still, the capacitance retention of 50.4% at 75 °C is greater than those at lower temperatures (29.7% at 0 °C, 39.1% at 25 °C and 42.6% at 50 °C). These results can be rationalized by the enhanced mobility of the ions in the electrolyte at high temperature. Thus, the ions would penetrate into the interior surfaces of MnO_2 more easily, promoting more charge accumulation and transfer.

The electrochemical performance was further investigated by galvanostatic charging/discharging technique. Fig. 4 shows the charging/discharging curves of each temperature at current densities of 1 A g^{-1}, 2 A g^{-1}, 4 A g^{-1} and 8 A g^{-1}. At temperatures no more than 50 °C, it is observed that these curves show very symmetric triangular shapes, revealing a good pseudo-capacitive behavior and a highly reversible Faradic reaction of MnO_2. At high temperature of 75 °C, obvious voltage plateaus related to the electrochemical polarization occur on the charging curves, especially at the low current density of 1 A g^{-1}. The irreversible behavior results in a low coulombic efficiency (CE). The values of SC and CE are calculated and given in Table 1. The SC values are consistent with the CV results. The composites electrodes have a high CE of >98% at temperatures of 0 °C and 25 °C. As the temperature increases over 50 °C, the CE decreases with increasing temperature or decreasing current density. Additionally, a voltage jump, or called IR drop, is observed at the beginning of the discharging curve, which is associated with the internal resistance of capacitor. Fig. 5 plots the dependence of IR drop on the current density, the slope of which can be used to estimate the internal resistance of the capacitor. Generally, a greater slope implies a larger internal resistance of the capacitor. It is obviously from Fig. 5 that the internal resistance increases with the decrease in the temperature, suggesting a better rate performance at higher temperature.

Table 1
Specific capacitance (SC) and coulombic efficiency (CE) of MnO_2@CNF at each set of temperature.

Current density (A/g)	0 °C		25 °C		50 °C		75 °C	
	SC (F g^{-1})	CE[a] (%)	SC (F g^{-1})	CE (%)	SC (F g^{-1})	CE (%)	SC (F g^{-1})	CE (%)
1	365	99.5	426	98.5	509	87.8	546	61.4
2	357	99.1	416	98.9	481	95.6	527	69.9
4	329	99.4	397	99.1	429	97.2	487	75.9
8	278	100	355	99.5	376	98.6	420	91.8

[a] The coulombic efficiency (CE) is defined by CE (%) = discharge capacity/charge capacity.

Electrochemical impedance spectroscopy (EIS) measurement was used to gain insight into the temperature dependence of the resistive and pseudo-capacitive behaviors on the performance of the supercapacitor. Fig. 6 shows the resulting Nyquist spectra of the electrodes at different temperatures from 0 °C to 75 °C, all of which consist of a compressed arc in the high-frequency range and a sloped line in the low-frequency region. A simple equivalent circuit model can be built to analyze these impedance spectra, as shown in the inset of Fig. 6. The first intercept of the arc on the real axis presents the value of the ohmic resistance of electrolyte and the internal resistance of the active materials and is denoted as R_s. The impedance arc in the high-frequency region can be modeled by an interfacial Faradic charge transfer resistance (R_{ct}) and a parallel

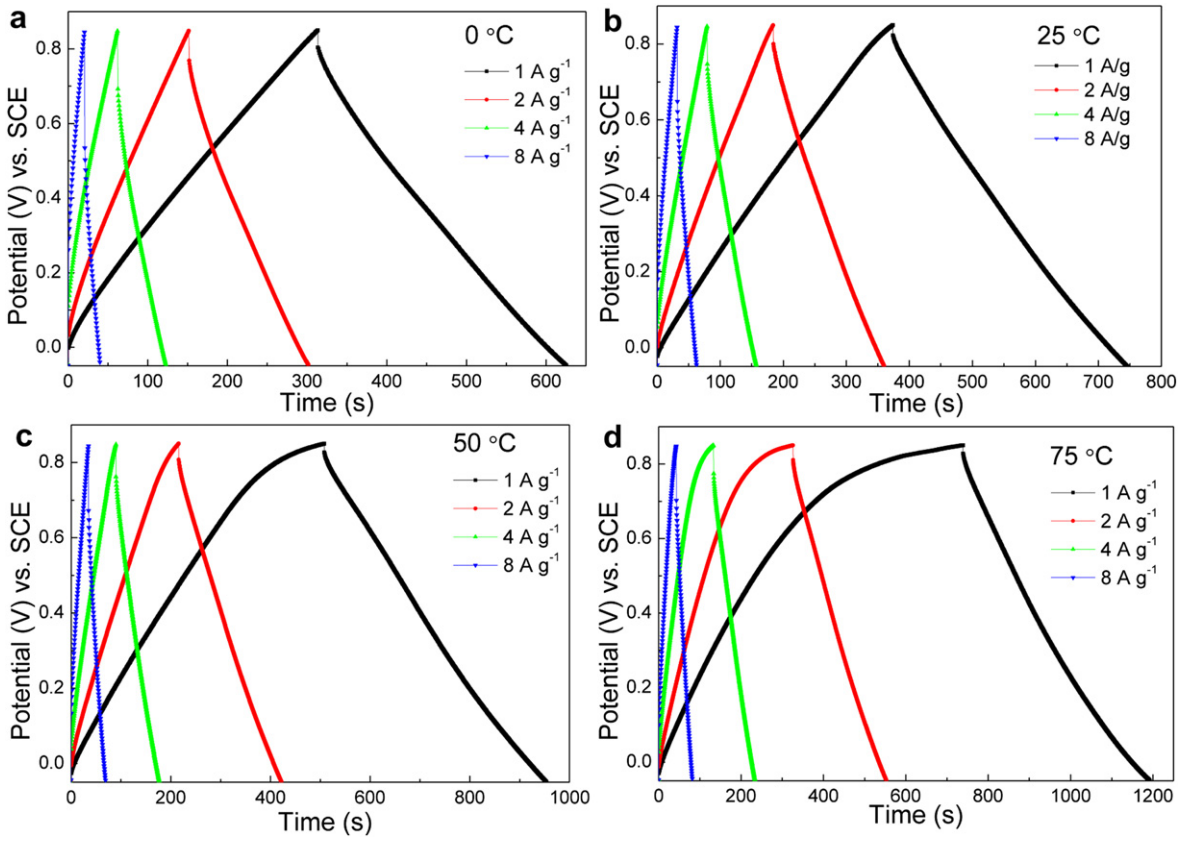

Fig. 4. Galvanostatic charging/discharging curves of MnO_2@CNF composites electrodes tested at (a) 0 °C; (b) 25 °C; (c) 50 °C and (d) 75 °C.

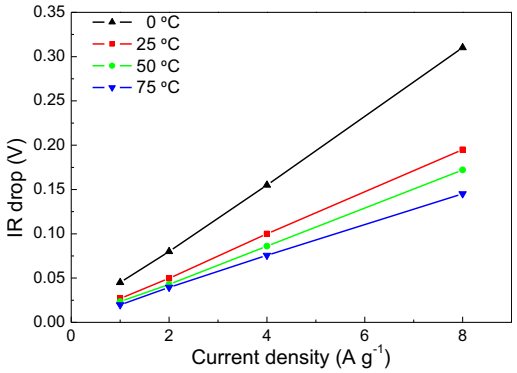

Fig. 5. Dependence of IR drop on the discharging current density at different temperatures.

constant phase element (CPE) in place of double layer capacitance. Following the arc, the straight line with a slope of 45° in the medium frequency represents the finite-length diffusion Warburg impedance (Z_w), which is associated with electrolyte ions diffusion/transport throughout the electrode [13]. The vertical line in the very low-frequency region is an indication of ideally capacitive behavior mainly from the pseudocapacitance of MnO_2. The primary fitting results are given in Table 2. It can be seen that both R_s and R_{ct} decrease with the increase in the temperature from 0 °C to 75 °C, indicating a lower internal resistance and a faster kinetics of Faradaic reaction at higher temperature. The decrease is rationalized by an increase in the ionic conductivity of electrolyte due to the enhanced mobility of the ions in the electrolyte with the increase in the temperature. Additionally, the gradually increased slope of the line in the low-frequency with the increasing temperature suggests a better capacitive performance and a lower diffusion resistance at higher temperature (Fig. 6).

The cycling capability is an important factor in determining the supercapacitor electrodes for practical applications. A vast mass of literatures have demonstrated that MnO_2-based electrodes exhibited excellent cycling stability at room temperature. However, scarcely did these reports study their cycling performance at high temperature. In fact, the phase structure and morphology of MnO_2-based materials, unlike the carbonaceous materials, are highly susceptible to the high temperature, which may lead to a significant capacitance variation. The present study compares the cycling

Table 2
The fitting results of R_s and R_{ct} of MnO_2@CNF electrodes at different temperatures.

Resistance	0 °C	25 °C	50 °C	75 °C
R_s (Ω)	8.9	5.6	4.9	3.9
R_{ct} (Ω)	2.5	1.1	0.8	0.7

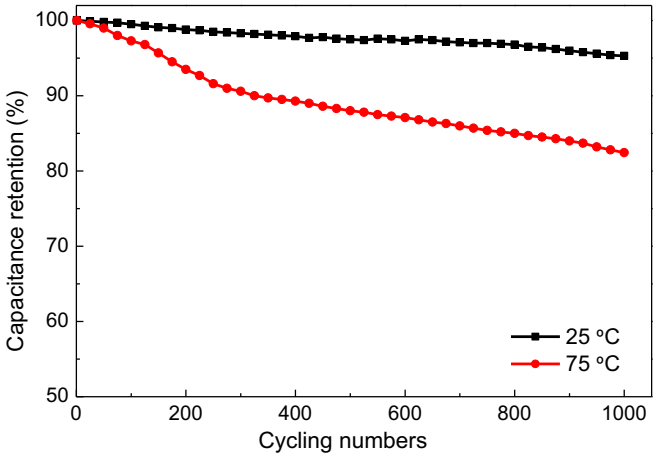

Fig. 7. Cycling stability of MnO_2@CNF composites at different temperatures.

stability of MnO_2@CNF electrodes at 25 °C and 75 °C. Fig. 7 shows the resulting normalized capacitance retention tested at 10 A g^{-1} over 1000 cycles. At low temperature of 25 °C, the electrode has good capacitance retention of 95.3%, showing excellent cycling stability just as those reported at room temperature. By contrast, it can be seen that the electrode lose 18.6% of its initial capacitance after the cycling test at 75 °C. The deterioration in the capacitance is related to the dissolution of MnO_2 or the mechanical and electrical faults between MnO_2 and CNFs. After 1000 cycles, we observe the colorless electrolyte have changed into yellowish color, which is an obvious evidence of the dissolution of MnO_2. Nevertheless, the yellowish color at 25 °C is much lighter than that at 75 °C, indicating the electrode has a more serious dissolution at high temperature. This observation is in good agreement with the polarization, as discussed earlier. The phase structure and the morphology of the electrode after 1000 cycles have been characterized by XRD and FESEM. As shown in Fig. 8, birnessite-type MnO_2 preserves when cycling at

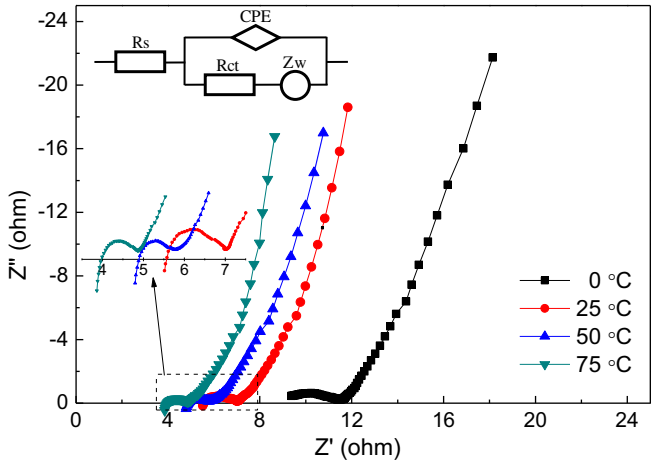

Fig. 6. Nyquist plots of MnO_2@CNF composites at different temperatures. Inset is the corresponding equivalent circuit.

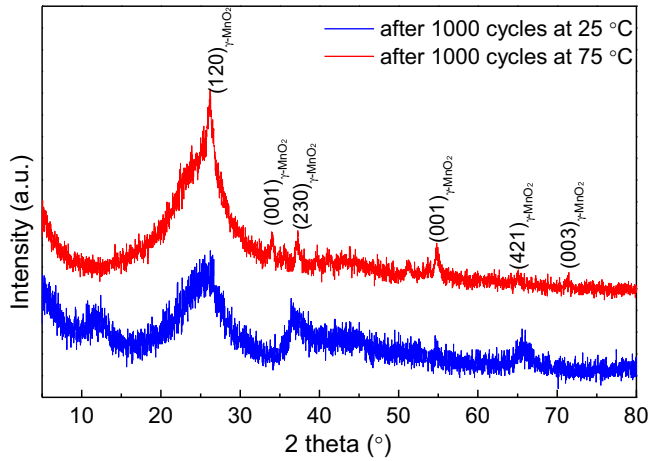

Fig. 8. XRD patterns of MnO_2@CNF composites after 1000 cycles at 25 °C and 75 °C.

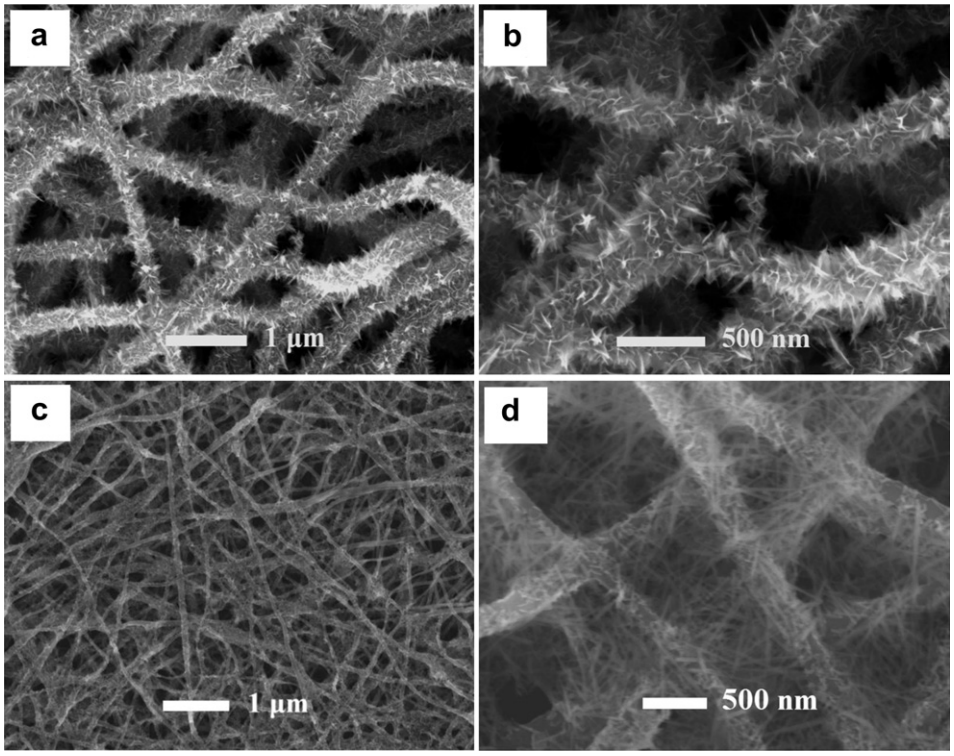

Fig. 9. SEM images of MnO_2@CNF composites after 1000 cycles at 25 °C (a and b) and 75 °C (c and d).

25 °C but evolves to a new phase of γ-MnO_2 at 75 °C. The γ-MnO_2 has been proven to show inferior specific capacitance to birnessite-type MnO_2 [28]. Fig. 9 shows the morphology of the electrodes cycling at 25 °C and 75 °C. It is found that hierarchical MnO_2 nanoflakes are still well-maintained on the CNFs at 25 °C and the integral structure of the electrode remains, while MnO_2 nanorods are formed at 75 °C having a loose mechanical connection to or even detachment from the CNFs. We believe the significant loss in the pseudocapacitance of MnO_2 at high temperature is attributed not only to its dissolution into electrolyte but also to its phase transition and morphological change.

4. Conclusions

A hierarchical coaxial architecture consisting of nanoflaky MnO_2 layers and highly conductive carbon nanotubes-embedded carbon nanofibers has been prepared as freestanding electrodes to study the temperature-dependent pseudo-capacitive properties of MnO_2 in mild Na_2SO_4 electrolyte. The MnO_2@CNF composites exhibit excellent electrochemical performance at temperatures ranging from 0 °C to 75 °C. An increasing temperature leads to an enhanced specific capacitance, a better rate capability but a reduced coulombic efficiency. The composites show good cycling stability of 95.3% at 25 °C and inferior capacity retention of 82.4% at 75 °C. The birnessite-type MnO_2 nanoflakes are found to evolve to γ-MnO_2 nanorods during cycling test at high temperature. The temperature-dependent studies offer a fundamental understanding of the pseudo-capacitive behavior of MnO_2 for supercapacitor applications.

Acknowledgments

The authors acknowledge the fund from the National Natural Science Foundation of China (No. 50972065 and No. 51102143) and New Teachers Fund for Doctor Stations (20100002120006, Ministry of Education). We also appreciated the financial support from Guangdong Province Innovation R&D Team Plan.

References

[1] B.E. Conway, Electrochemical Supercapacitors: Scientific Fundamentals and Technological Applications, KluwerAcademic/Plenum Publishers, New York, 1999.
[2] P. Simon, Y. Gogotsi, Nat. Mater. 7 (2008) 845–854.
[3] Y. Zhai, Y. Dou, D. Zhao, P.F. Fulvio, R.T. Mayes, S. Dai, Adv. Mater. 23 (2011) 4828–4850.
[4] L.L. Zhang, X.S. Zhao, Chem. Soc. Rev. 38 (2009) 2520–2531.
[5] G. Wang, L. Zhang, J. Zhang, Chem. Soc. Rev. 41 (2012) 797–828.
[6] J. Liu, J. Jiang, C. Cheng, H. Li, J. Zhang, H. Gong, H.J. Fan, Adv. Mater. 23 (2011) 2076–2081.
[7] X. Lu, T. Zhai, X. Zhang, Y. Shen, L. Yuan, B. Hu, L. Gong, J. Chen, Y. Gao, J. Zhou, Y. Tong, Z.L. Zhong, Adv. Mater. 24 (2012) 938–944.
[8] J. Liu, J. Jiang, M. Bosman, H.J. Fan, J. Mater. Chem. 22 (2012) 2419–2426.
[9] W. Wei, X. Cui, W. Chen, D.G. Ivey, Chem. Soc. Rev. 40 (2011) 1697–1721.
[10] S.W. Zhang, G.Z. Chen, Energy Mater. 3 (2008) 186–200.
[11] Z. Li, J. Wang, S. Liu, X. Liu, S. Yang, J. Power Sources 196 (2012) 8160–8165.
[12] J.H. Kim, K.H. Lee, L.J. Overzet, G.L. Lee, Nano Lett. 11 (2011) 2611–2617.
[13] J. Yan, Z. Fan, T. Wei, W. Qian, M. Zhang, F. Wei, Carbon 48 (2010) 3825–3833.
[14] L. Bao, J. Zang, X. Li, Nano Lett. 11 (2011) 1215–1220.
[15] R. Liu, J. Duay, S.B. Lee, ACS Nano 5 (2011) 5608–5619.
[16] P. Liu, M. Verbrugge, S. Soukiazian, J. Power Sources 156 (2006) 712–718.
[17] P. Kotz, M. Hahna, R. Gallay, J. Power Sources 154 (2006) 550–555.
[18] C. Masarapu, H.F. Zeng, K.H. Hung, B. Wei, ACS Nano 3 (2010) 2199–2206.
[19] X.R. Liu, G. Peter, P.G. Pickup, Energy Environ. Sci. 1 (2008) 494–500.
[20] J. Yan, E. Khoo, A. Sumboja, P.S. Lee, ACS Nano 4 (2010) 4247–4255.
[21] J.G. Wang, Y. Yang, Z.H. Huang, F. Kang, Electrochim. Acta 75 (2012) 213–219.
[22] X. Jin, W. Zhou, S. Zhang, G.Z. Chen, Small 3 (2007) 1513–1517.
[23] Y. Yang, A. Centrone, L. Chen, F. Simeon, T.A. Hatton, G.C. Rutledge, Carbon 49 (2011) 3395–3403.
[24] H. Xia, M. Lai, L. Lu, J. Mater. Chem. 20 (2010) 6896–6902.
[25] K.W. Nam, K.B. Kim, J. Electrochem. Soc. 153 (2006) A81–A88.
[26] C. Julien, M. Massot, R. Baddour-Hadjean, S. Franger, S. Bach, J.P. Pereira-Ramos, Solid State Ionics 159 (2003) 345–356.
[27] L.L. Zhang, T. Wei, W. Wang, X.S. Zhao, Microporous Mesoporous Mater. 123 (2009) 260–267.
[28] O. Ghobane, J.L. Pascal, B. Fraisse, F. Favier, ACS Appl. Mater. Interfaces 2 (2010) 3493–3505.